Supporting information for: Regulation and Plasticity of Catalysis in Enzymes: Insights from Analysis of Mechanochemical Coupling in Myosin

Xiya Lu,[†] Victor Ovchinnikov,[‡] Darren Demapan,[†] Daniel Roston,[†] and Qiang Cui[*,†]

†*Department of Chemistry and Theoretical Chemistry Institute, University of Wisconsin-Madison, 1101 University Avenue, Madison, WI 53706*

‡*Department of Chemistry and Chemical Biology, Harvard University, 12 Oxford St., Boston, MA 02138*

E-mail: cui@chem.wisc.edu

1 Collective Variables in the Metadynamics Simulations

Collective variables used in the metadynamics simulations include the anti-symmetric stretch, $P_\gamma O_{3\beta} - P_\gamma O^{W1}$, and the ζ coordinate[S1] that describes the proton transfers. Due to the collective nature of ζ, it is capable of describing proton transfers without explicitly specifying the number and identity of the groups that mediate proton transfer. Therefore, it is well suited for discovering proton transfer pathways in a nearly automated fashion. In certain cases, to turn off undesirable proton transfer pathways, specific sidechains are treated by

a MM rather than a QM model. In particular, for the W2 and the S181-W2 mechanisms, Glu459 and Arg238 are treated as MM to avoid Glu459 from accepting a proton. Note, however, that a larger and *identical* QM region is used for all mechanisms (see Methods in the main text) in the subsequent string calculations. The identity of proton donor, acceptor and potential proton shuttling group used in the definition of ζ for different pathways are listed in Table 1.

Table S1: Identity of proton donor, acceptor and potential proton shuttling group used in the definition of ζ in the metadynamics simulations of different reaction pathways.

Structural model	Pathway	Proton Donor	Proton Acceptor	Proton Shuttling groups
pre-powerstroke	W2-E459	P_β	Glu459 OE1	W1, W2, E459, ATP
pre-powerstroke	W2	P_β	Glu459 OE1	W1, W2, ATP
pre-powerstroke	W2-S181	P_β	Glu459 OE1	W1, W2, S181, ATP
pre-powerstroke	S236	P_β	Arg238 CZ	W1, S236, ATP
pre-powerstroke	S236-W3-S181	P_β	Glu459 OE1	W1, W3, S236, S181, ATP
post-rigor	S236	P_β	Arg238 CZ	W1, S236, ATP
"closed" post-rigor	W2-E459	P_β	Glu459 OE1	W1, W2, E459, ATP

2 The Projection Problem in Metadynamics Simulations for Myosin

The advantage of using the ζ coordinate, which is highly collective in nature, is that metadynamics simulations can be used to automatically discover reaction pathways with little prior input. On the other hand, the collective nature of ζ also introduces uncertainty in the computed 2D free energy surface, since rather different reactive configurations (which likely have very different energies) can be mapped onto the same location on the low-dimensional manifold. In this section, we use the S236 pathway in the pre-powerstroke state as an example to illustrate such projection problem in the metadynamics simulations; this type of problem is observed for all pathways studied here, while the S236 pathway is chosen here due to its simplicity in the nature of transition state.

Figs. 1c-d show two examples, which correspond to a structure close to the final hydrolysis product and transition state, respectively. They share similar values for the set of collective coordinates: the $P_\gamma O_{3\beta}$ – $P_\gamma O^{W1}$ is 0.8 $\sim$ 1.0 Å and ζ is $\sim$ 0.0. Energetically, the configure close to the product is far more stable than the transition state, so Gaussian potentials keep being deposited to this region during metadynamics simulations, skewing the free energy surface. Indeed, the free energy barrier found by metadynamics is $\sim$ 30 kcal/mol, which is 5 kcal/mol higher than the value from the string calculations.

Moreover, as Gaussian potentials accumulate in the region close to the product region, the system is driven away from the minimum free energy pathway during metadynamics simulations. In Fig. 1a, the free energy surface is superimposed with a reactive trajectory observed in metadynamics simulation; in Fig. 1b, the same free energy surface is superimposed with the converged string projected onto the two-dimensional space. Clearly, the two pathways are distinct: while P_γ-$O_{3\beta}$ breaks prior to proton transfer in the converged string, the metadynamics simulation leads to a reactive trajectory that follows the opposite sequence of event and transverses the high energy region of the free energy surface.

These observations highlight that free energy calculations using metadynamics should be treated with great care when projecting high-dimensional processes onto a low-dimensional space.

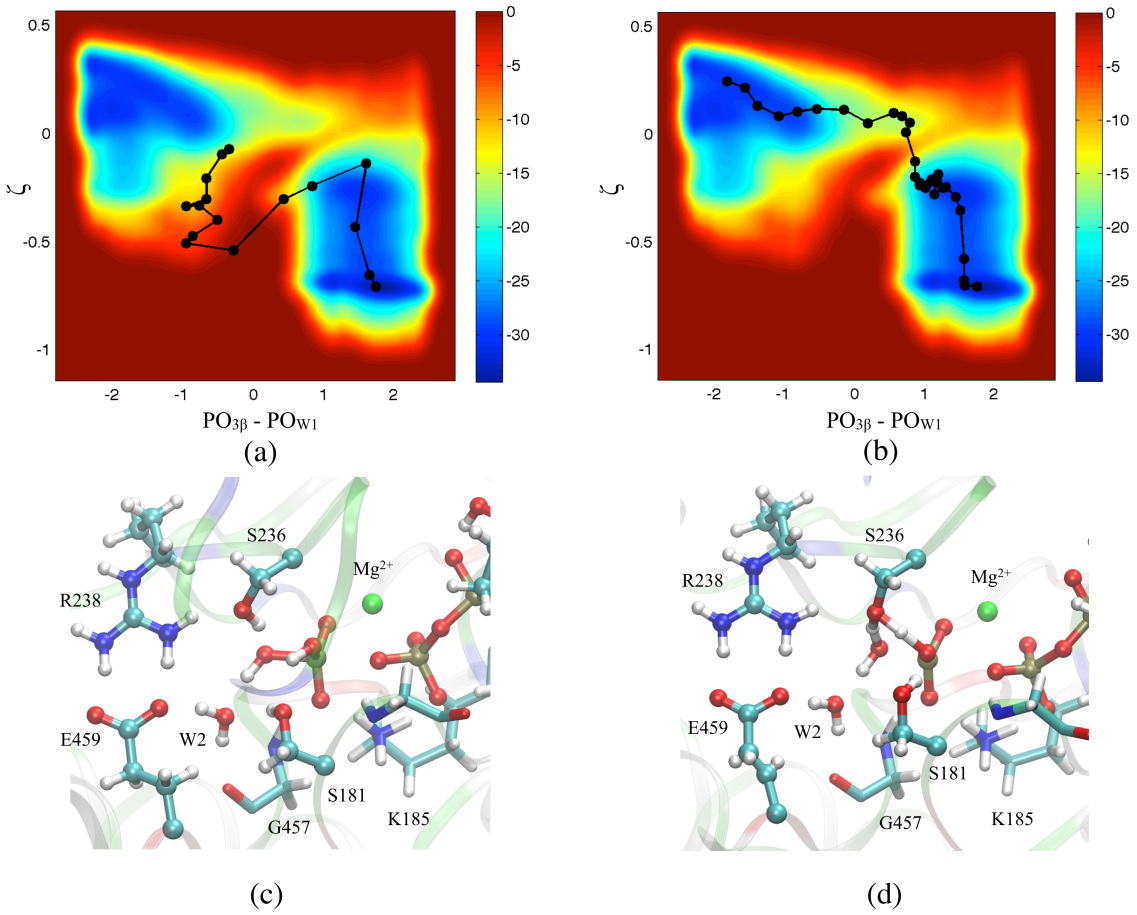

Figure S1: The 2D free energy surface shown in (a)(b) is obtained from metadynamics for S236 pathway in the pre-powerstroke state. (a) The reactive trajectory is projected on the surface as the solid black line. The structures in the reactive trajectory are used as the initial guess in the following string calculation. (b) The converged string is illustrated on the surface as the solid black line. Each circle corresponds to an image along the string. The color scale denotes free energy in the unit of kcal/mol. (c) The representative pre-product structure in which hydroxyl group in the inorganic phosphate is about to rotate towards to ADP. (d) The desired transition state discovered in the MFEP in the string method.

3 Collective Variables in the String Calculations

Collective variables used in the string calculations are summarized in Table 2.

Table S2: Definition of the collective variables in the string method

System	Mechanism	Collective variable
pre-powerstroke	W2-E459	d(W1 O-ATP P_γ), d(ATP P_γ-ATP $O_{3\beta}$), d(W2 H_1-ATP $O_{2\gamma}$), d(W2 H_1-ATP $O_{3\beta}$), d(W1 O-W1 H_1), d(W1 O-W1 H_2), d(W2 O-W2 H_1), d(W2 O-W2 H_2), d(W1 H_1-W2 O), d(W1 O-W2 O), d(W2 H_2-E459 OE1), d(ATP P_β-ATP $O_{3\beta}$), d(Mg-ATP $O_{1\gamma}$), d(Mg-ATP $O_{1\beta}$), d(E459 OE1-R238 HH11), d(E459 OE2-R238 HH21)
pre-powerstroke	W2[a]	d(W1 O-ATP P_γ), d(ATP P_γ-ATP $O_{3\beta}$), d(W1 H_1-ATP $O_{2\gamma}$), d(W1 H_1-ATP $O_{3\beta}$), d(W1 O-W1 H_1), d(W1 O-W1 H_2), d(W2 O-W2 H_1), d(W2 O-W2 H_2), d(W1 H_1-W2 O), d(W1 O-W2 O), d(W2 H_2-E459 OE1), d(ATP P_β-ATP $O_{3\beta}$), d(Mg-ATP $O_{1\gamma}$), d(Mg-ATP $O_{1\beta}$), d(E459 OE1-R238 HH11), d(E459 OE2-R238 HH21)
pre-powerstroke	W2-S181	d(W1 O-ATP P_γ), d(ATP P_γ-ATP $O_{3\beta}$), d(S181 HG1-ATP $O_{2\gamma}$), d(S181 HG1-ATP $O_{3\beta}$), d(W1 O-W1 H_1), d(W1 O-W1 H_2), d(W2 O-W2 H_1), d(W2 O-W2 H_2), d(W1 H_1-W2 O), d(W1 O-W2 O), d(W2 H_2-E459 OE1), d(W2 H_1-G457 O), d(W2 H_1-S181 OG), d(S181 OG-S181 HG1), d(ATP P_β-ATP $O_{3\beta}$), d(Mg-ATP $O_{1\gamma}$), d(Mg-ATP $O_{1\beta}$), d(E459 OE1-R238 HH11), d(E459 OE2-R238 HH21)
pre-powerstroke	S236	d(W1 O-ATP P_γ), d(ATP P_γ-ATP $O_{3\beta}$), d(S236 HG1-ATP $O_{2\gamma}$), d(S236 HG1-ATP $O_{3\beta}$), d(W1 O-W1 H_1), d(W1 O-W1 H_2), d(W1 O-W2 O), d(W1 H_2-W2 O), d(W1 H_1-S236 OG), d(S236 OG-S236 HG1), d(ATP P_β-ATP $O_{3\beta}$), d(Mg-ATP $O_{1\gamma}$), d(Mg-ATP $O_{1\beta}$)
pre-powerstroke	S236-W3-S181	d(W1 O-ATP P_γ), d(ATP P_γ-ATP $O_{3\beta}$), d(S181 HG1-ATP $O_{2\gamma}$), d(S181 HG1-ATP $O_{3\beta}$), d(W1 O-W1 H_1), d(W1 O-W1 H_2), d(W1 O-W2 O), d(W1 H_2-W2 O), d(W1 H_1-S236 OG), d(S236 OG-S236 HG1), d(S236 HG1-W3 O), d(W3 O-W3 H_1), d(W3 O-W3 H_2), d(W3 H_2-S181 OG), d(S181 OG-S181 HG1), d(ATP P_β-ATP $O_{3\beta}$), d(Mg-ATP $O_{1\gamma}$), d(Mg-ATP $O_{1\beta}$)
post-rigor	S236	d(W1 O-ATP P_γ), d(ATP P_γ-ATP $O_{3\beta}$), d(S236 HG1-ATP $O_{2\gamma}$), d(S236 HG1-ATP $O_{3\beta}$), d(W1 O-W1 H_1), d(W1 O-W1 H_2), d(W1 H_1-S236 OG), d(S236 OG-S236 HG1), d(ATP P_β-ATP $O_{3\beta}$), d(Mg-ATP $O_{1\gamma}$), d(Mg-ATP $O_{1\beta}$)
"closed" post-rigor	W2-E459	d(W1 O-ATP P_γ), d(ATP P_γ-ATP $O_{3\beta}$), d(W1 H_1-ATP $O_{2\gamma}$), d(W1 H_1-ATP $O_{3\beta}$), d(W1 O-W1 H_1), d(W1 O-W1 H_2), d(W2 O-W2 H_1), d(W2 O-W2 H_2), d(W1 H_1-W2 O), d(W1 O-W2 O), d(W2 H_1-E459 OE1), d(W2 O-E459 CD), d(ATP P_β-ATP $O_{3\beta}$), d(Mg-ATP $O_{1\gamma}$), d(Mg-ATP $O_{1\beta}$), d(E459 OE1-R238 HH11), d(E459 OE2-R238 HH21)
"closed" post-rigor	water reorganization	d(W1 O-ATP P_γ), d(W2 O-ATP P_γ), d(W1 O-W2 O), d(W2 H_1-E459 OE1), d(W2 O-E459 CD), d(W2 H_2-G457 O)

[a] a NOE constraint is applied to the distance between W2 water and Glu459 to prevent a proton from being too close to the Glu459.

4 Comparison between Metadynamics and String Calculations for the W2-E459 Pathway in the Pre-powerstroke State

The minimum free energy path (MFEP) computed by string method in this work does not capture contributions due to the thermal fluctuations of the CVs orthogonal to the string. Therefore, too few number of CVs in MFEP calculations do not properly describe the reactive process, while too many CVs might potentially freeze out the relevant degrees of freedom. In this section, we use the W2-E459 pathway to demonstrate that the string method arrives at the same pathway and free energy barrier with metadynamics simulations if the projection problem in metadynamics discussed in Sect. is properly handled. To remove the contamination due to the product-like structures shown in Fig. 1c, a strong harmonic restraint is applied to the ζ coordinate to enforce it to be positive; this helps prevents metadynamics from sampling the pre-product configuration (with a positive ζ, the excess charge does not reach γ-phosphate), so reliable structure and energetics are obtained for the TS (which shares similar ζ as pre-product configurations). As seen in Fig. 2, the converged string projected onto the 2D space closely follows the free energy valley computed by metadynamics simulations. The two approaches also give similar free energy barrier of $\sim$17 kcal/mol. Therefore, entropic effects associated with the fluctuations of CVs orthogonal to the string do not appear to play a major role in the current problem.

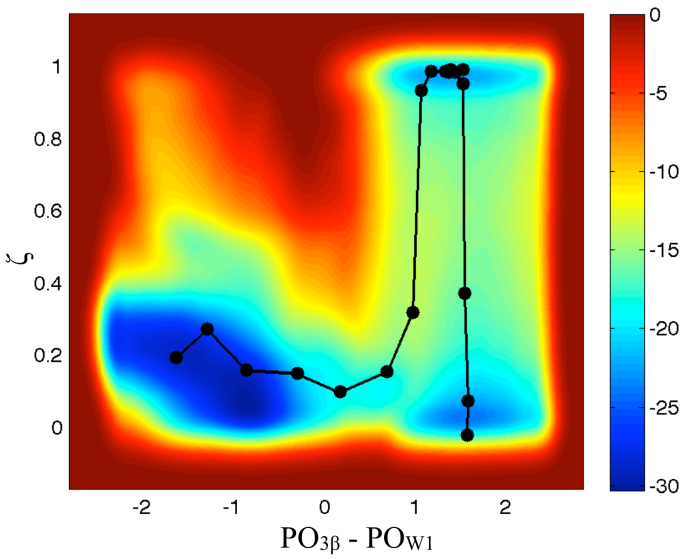

Figure S2: The 2D free energy surface obtained from metadynamics for W2-E459 pathway in the pre-powerstroke state. The converged string is illustrated on the surface as the solid black line. Results obtained from metadynamics and string match each other well regarding to the mechanism and free energy barrier. Each circle corresponds to an image along the string. The color scale denotes free energy in the unit of kcal/mol.

5 Electrostatic Polarization due to Glu459 is Captured by a Simple Model

To illustrate the impact of electrostatic polarization due to Glu459 on the proton transfers, we construct a simple gas phase model (Fig. 3). The model consists of one acetate group and two water molecules (referred to as the two-water model) or three water molecules (referred to as the three-water model), and we study the proton transfer from the first water (W1) to the second water (W2). The positions of the water molecules and acetate are adjusted to allow hydrogen bonding interactions of typical distances; a fixed MM point charge is placed next to W1 to stabilize the hydroxide in the product state. The proton transfer is studied by conducting one-dimensional adiabatic mapping at the DFTB3 level; the reaction coordinate is the antisymmetric stretch involving the breaking O^{W1}-H bond and forming O^{W2}-H bond. The transition state is approximated by the highest energy structure along the adiabatic

mapping profile. Single point energy calculations at the B3LYP/aug-cc-pVTZ level are also carried out for comparison.

At the DFTB3 level, the barrier height is 4.8 kcal/mol for the two-water model and substantially higher (14.1 kcal/mol) for the three-water model; the exothermicity of the reaction is similar, -1.0 kcal/mol and +2.3 kcal/mol for the two-water and three-water model, respectively. The values are similar at the B3LYP level; for example, the barrier heights are 6.5 kcal/mol and 16.0 kcal/mol, respectively; the favorable comparison of these values to the corresponding DFTB3 values of 4.8 and 14.1 kcal/mol further supports the use of DFTB3 for the description of the relevant proton transfer steps in the myosin problem. Therefore, it is evident that direct stabilization of the hydronium-like species by acetate in the two-water model reduces the proton transfer barrier significantly; i.e., the stabilization effect of the acetate is quenched significantly when a water molecule separates the acetate and the hydronium-like species. Moreover, if the acetate is treated classically using a MM model, the barrier height in the two-water model is increased by less than 1 kcal/mol, demonstrating that stabilization of the transition state is not due to charge transfer.

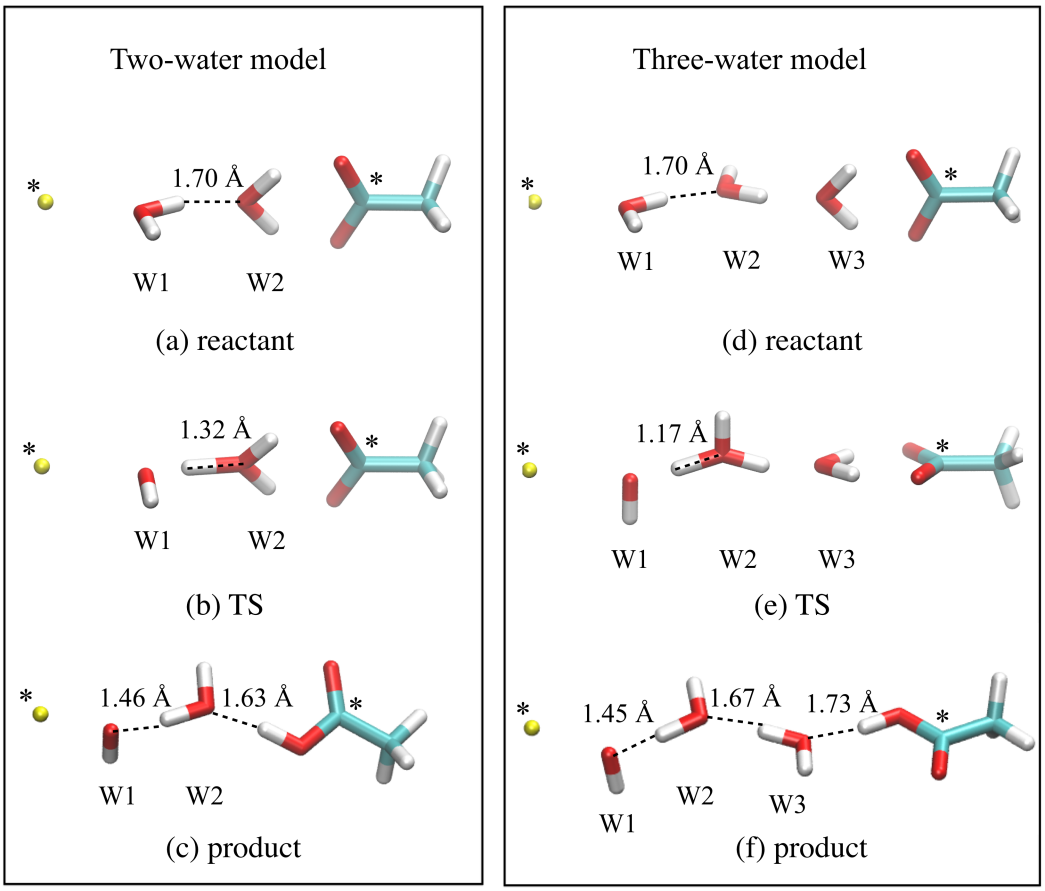

Figure S3: Proton transfer in a model system consisting of acetate and water molecules to illustrate the impact of polarization effects. The acetate and water molecules are colored by atom type, and the MM point charge is colored in yellow. Atoms fixed are denoted by asterisk. (a) - (c) Snapshots for the reactant, transition state and product in the two-water model, respectively. (d) - (f) Snapshots for the reactant, transition state and product in the three-water model, respectively.

6 Calibration of DFTB3 with B3LYP calculations

Previous benchmark calculations[S2] and recent applications[S3,S4] indicate that the DFTB3 approach provides a semi-quantitative description for phosphoryl transfer reactions, including key structural, energetic and vibrational features of phosphoryl transition states. Results for the model proton transfer reactions reported in the last section further supports the use of DFTB3 for the description of relevant proton transfer steps. Nevertheless, the DFTB3 model

is not quantitatively accurate for complex reactions that involve highly charged species like ATP hydrolysis. To ensure that key trends observed in the free energy profiles are meaningful, we conduct B3LYP and B3LYP/MM calculations for model reactions in the gas phase, solution and the real enzyme system.

6.1 Exothermicity of Hydrolysis

The free energy simulations indicate that the hydrolysis reaction in the pre-powerstroke state is exothermic by about 10 kcal/mol, while experimental measurements indicate that the equilibrium constant for the hydrolysis step in this functional state is close to 1. Therefore, it is likely that the DFTB3 approach overestimates the exothermicity of the hydrolysis reaction by a substantial amount.

To verify this hypothesis, we study a model hydrolysis reaction in the gas phase; the corresponding reactant and product molecules are illustrated in Fig. 4. The reaction energy is evaluated by full geometry optimizations with DFTB3/3OB-OPhyd and the result is compared to B3LYP/aug-cc-pVTZ calculations (optimized at the respective levels). As shown in Table 3, the DFTB3/3OB-OPhyd model indeed overestimates the hydrolysis exothermicity by about 9 kcal/mol.

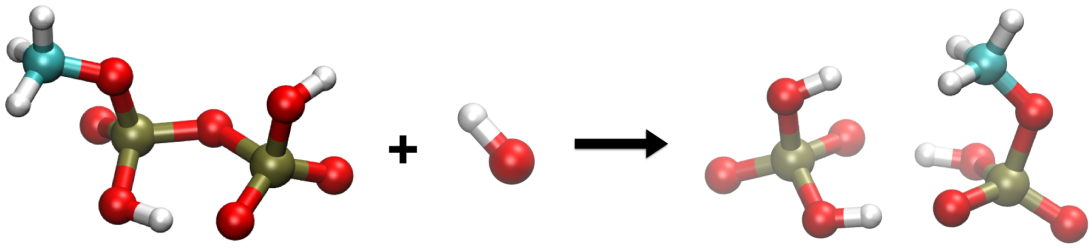

Figure S4: Model ADP hydrolysis reaction in the gas phase

Table S3: Energy difference between the product and the reactant in the model-ADP system obtained at DFTB3 and B3LYP/aug-cc-pvtz level in the unit of kcal/mol

Component	DFTB3/OPhyd	B3LYP/aug-cc-pvtz
OH^-	-2305.83	-47587.98
Model ADP^-	-19361.40	-785033.86
$(CH_3O)HPO_3^- + H_2PO_4^-$	-21681.65	-832627.19
Energy difference	-14.42	-5.35

6.2 Potential Energy Surface for the Hydrolysis Reaction in Solution

To further examine the applicability of the DFTB3/3OB-OPhyd model to the hydrolysis reaction of interest, we map the potential energy surface for the hydrolysis of a methyl triphosphate molecule bound to a Mg^{2+} ion in solution. Two-dimensional adiabatic mapping calculations are carried out using DFTB3/MM; several rounds of calculations are conducted to ensure that the water structures are thoroughly relaxed during the minimizations, which have a threshold in the RMS gradient of 0.01 kcal/mol/AA. Single point energy calculations are then carried out at the B3LYP/6-311++G(d,p)/MM level for comparison. The QM region in these calculations include the methyl triphosphate, the Mg^{2+} ion and its coordinating water molecules, the lytic water molecule and an additional 7 water molecules that stabilize the key charged groups. The MM region includes the rest of the water molecules in a droplet of 20 Å radius. We limit ourselves to adiabatic mapping calculations here because it's much more straightforward to compare DFTB3/MM and B3LYP/MM potential energy surfaces; it remains prohibitively expensive to conduct converged free energy surface at the B3LYP/MM level with a triplet-zeta plus polarization/diffuse functions basis set.

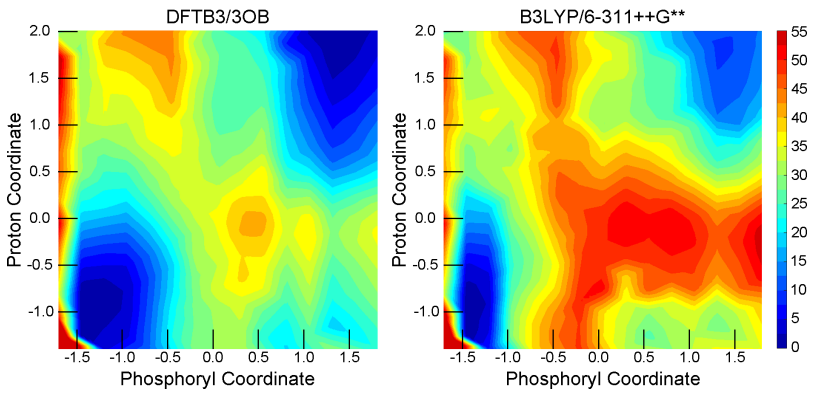

Figure S5: QM/MM potential energy scan of methyl triphosphate hydrolysis with concerted proton transfer using two different QM methods. Geometries were optimized at the DFTB3/3OB-OPhyd/MM level in explicit solvent (left) and those optimized geometries were used for single point calculations at the B3LYP/6-311++G**/MM level (right). The phosphoryl coordinate is defined as the difference in distance (in Å) between O^{lg}-P^{γ} and O^{nuc}-P^{γ}; the proton coordinate is defined as the difference in distance (in Å) between $O^{3\beta}$-H and O^{nuc}-H; thus reactants are on the lower left and products are on the upper right. The energy scale is in kcal/mol.

As shown in Fig.5, the key regions of the potential energy surface relevant to the concerted hydrolysis mechanism remain similar at the DFTB3/MM and B3LYP/MM levels. At the quantitative level, the exothermicity of the reaction is overestimated at the DFTB3/MM level by 9.4 kcal/mol, similar to the gas-phase benchmark shown in Table 3. Similarly, the barrier for the concerted mechanism is underestimated at the DFTB3/MM level by ∼6 kcal/mol. The region of the potential energy surface that corresponds to a highly asynchronous mechanism in which the phosphoryl transfer is completed prior to any significant proton transfer, the error in DFTB3/3OB-OPhyd/MM relative to B3LYP/MM is larger in magnitude and reaches more than 10 kcal/mol; this is consistent with our previous observation that the 3OB-OPhyd has remaining errors of ∼10 kcal/mol for dissociative mechanisms that involve three coordinated phosphorus.[S2] Although the magnitude of the error is large, it is systematic; since the transition states for different pathways discussed in the main text share a similar degree of P^{γ}-$O^{3\beta}$ cleavage and differ mainly in proton transfer routes, we expect that the qualitative trends for different pathways remain valid. This is supported by the test calculations observed in enzyme models discussed below.

6.3 Transition State Energetics in the Enzyme

As an attempt to calibrate the computed barrier heights in different pathways, we first conduct minimum energy path calculations at the DFTB3/MM level, and then compute single point energy calculations at the B3LYP/MM level for the barrier heights. Although these are not free energy barrier comparisons (which would be difficult to do at the B3LYP/MM level), the comparison provides qualitative indications regarding whether trends in the DFTB3/MM free energy barriers are meaningful.

As discussed extensively in previous studies,[S5–S8] MEP calculations in enzymes are sensitive to the protein environment used to initiate such calculations. Therefore, independent starting protein structures are selected for the MEP calculations; three snapshots from the reactant, TS and product regions of the W2-E459 pathway are used. The same starting protein structures are used to initiate MEP calculations for the different hydrolysis mechanisms, so that a fair comparison for the barrier heights can be made; otherwise, fluctuations in the MEP barrier height are likely too large to make the comparison meaningful. The MEP calculations are conducted using the zero-temperature string method implemented in CHARMM, and the transition state is further refined using conjugate peak refinement[S9] to obtain a precise estimate of the barrier height. The B3LYP/MM single point energy calculations are done with the 6-31+G(d,p) basis set, which was shown in previous studies[S10] to be of adequate accuracy for the current purpose.

As shown in Table 4, potential energy barrier heights from the MEP calculations at the DFTB3/MM level largely follow the same trend as the free energy barriers computed using the string method. With the same starting protein environment, the mechanisms that involve W2 have lower barriers than those involve S236. For the same mechanism, the potential barrier is lower when the protein environment is selected from MD simulations for the transition state; this is because the protein environment has reorganized to preferentially stabilize charge distributions characteristic of transition state structures.[S7]

The barrier heights computed at the B3LYP/MM level are generally higher and the differ-

ence from DFTB3/MM ranges from ∼2 kcal/mol to ∼10 kcal/mol; generally, the correction appears to be particularly large for the W2 mechanism. Therefore, it is evident that the DFTB3/MM approach is not yet quantitatively accurate for studying ATP hydrolysis in a complex enzyme like myosin. The encouraging aspect, however, is that the key trends are essentially maintained with the B3LYP/MM barrier heights: the W2-E459 and W2-S181 pathways feature barriers close to 20 kcal/mol, while the S236 and S236-W3-S181 pathways feature barriers close to be 30 kcal/mol; considering the large difference between DFTB3/MM and B3LYP/MM results for the W2 mechanism, it is difficult to conclude whether it should be considered as a low-barrier mechanism. Calculations at the B3LYP/MM level with more extensive sampling are required to better rank the W2 mechanism against others.

Table S4: Potential Energy Barriers from DFTB3/MM and B3LYP/6-31+G(d,p)/MM calculations for different reaction mechanisms in the pre-powerstroke state

Mechanism	Protein Environment		
	Reactant	Transition State	Product
W2-E459	15.4 (17.6), 17.5 (23.0)	11.0 (15.5), 10.0 (20.2)	14.8 (22.5)
W2-S181	19.1 (23.3)	15.7 (24.2)	17.5 (22.9)
W2	21.8 (32.2)	14.5 (26.9)	13.3 (24.7)
S236	25.0 (28.4)	20.9 (27.7)	23.8 (28.9)
S236-W3-S181	23.3 (30.1)	19.1 (28.6)	23.4 (29.3)

[a] The numbers without parentheses are at DFTB3 level, while the numbers with parentheses are single-point correction from B3LYP/6-31+G(d,p) on top of DFTB3 geometries.

7 Additional Results

7.1 Comparison of active site structure and fluctuations between the pre-powerstroke state and the closed post-rigor model

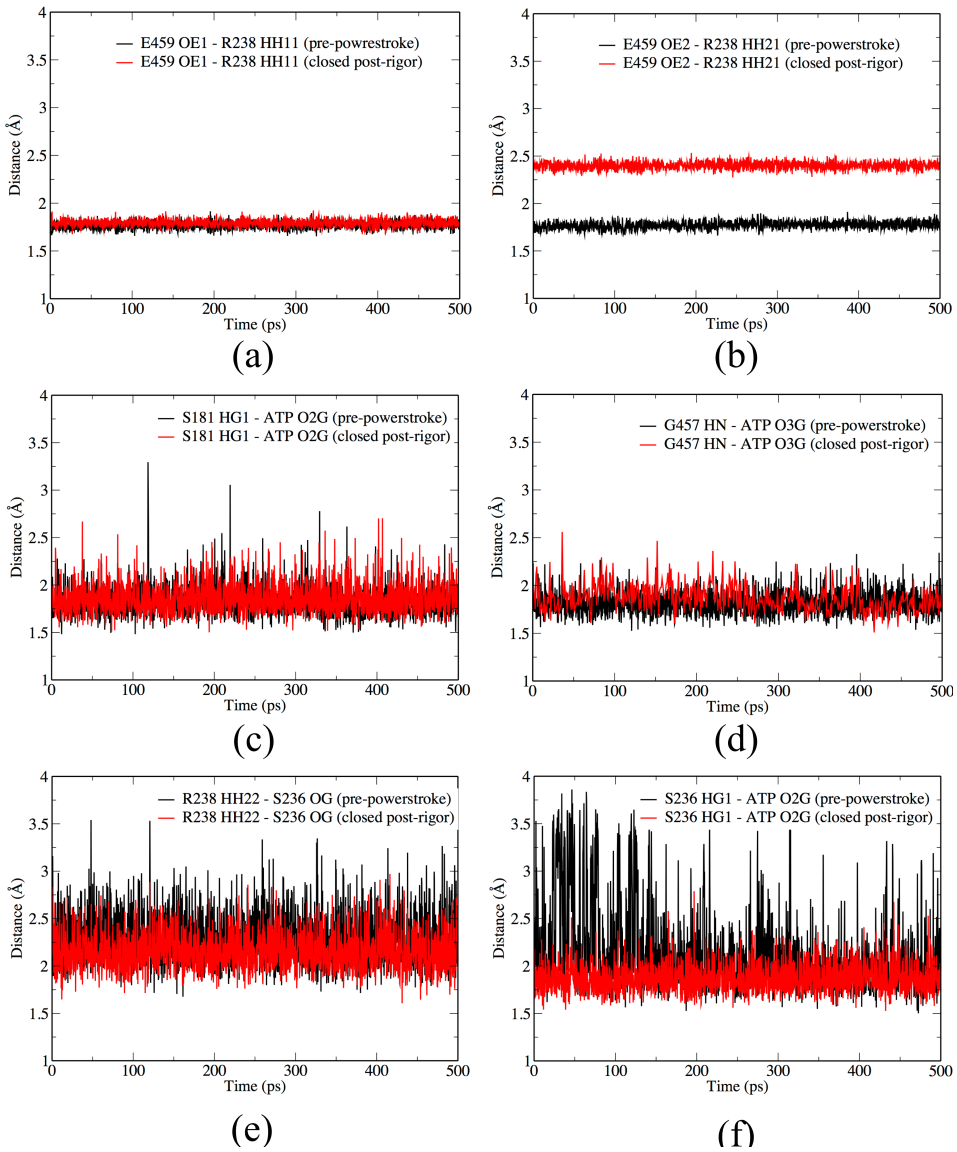

Figure S6: Distances between key residues in the reactant state

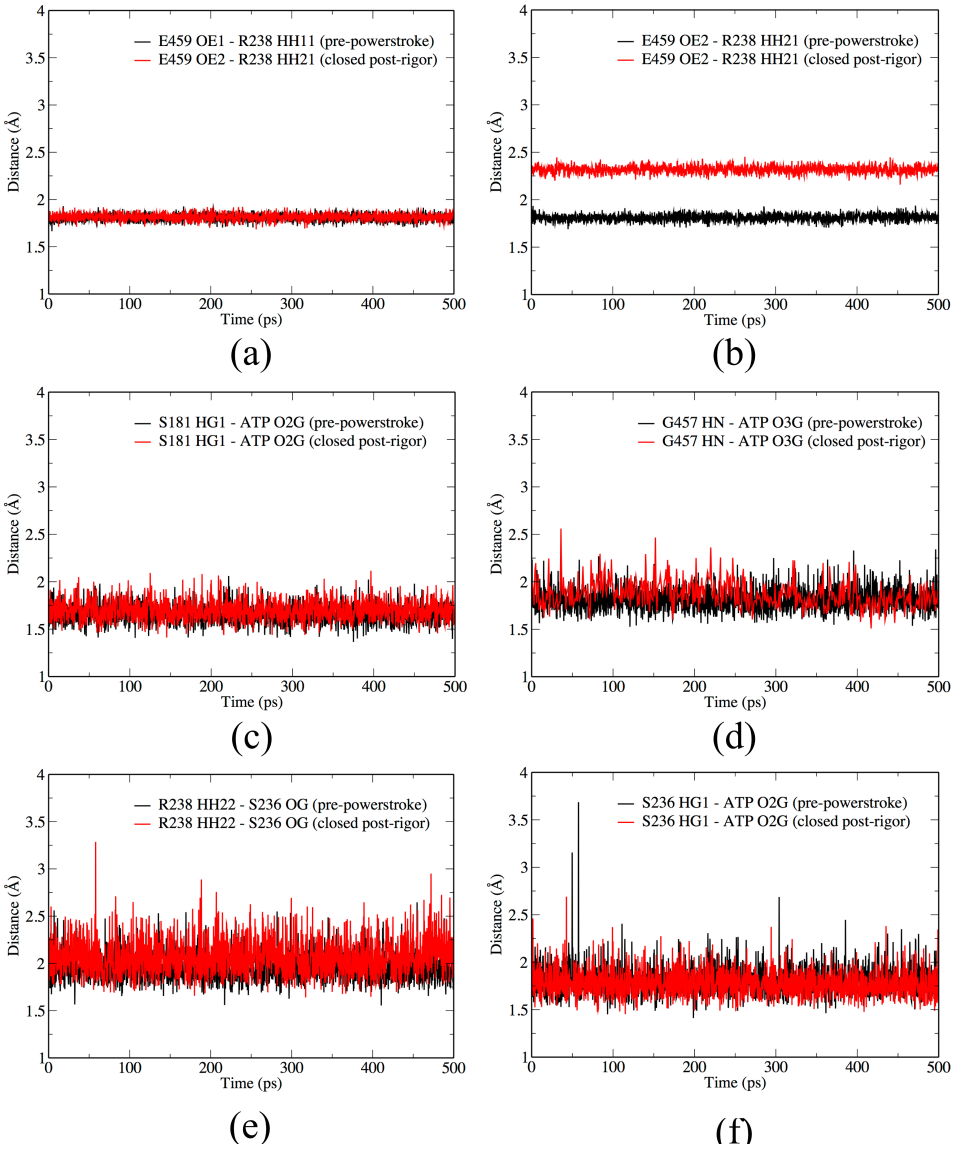

Figure S7: Distances between key residues in the transition state

7.2 RMSD between reaction pathways in the pre-powerstroke state and the closed post-rigor model

To better compare the reaction pathways in the two structural states, we calculate the RMSD between images along the optimized strings in the pre-powerstroke state and the closed post-rigor model. Both strings describe the W2-E459 mechanism, although there are structural (water) reorganizations in the initial stage for the closed post-rigor model (see discussion

in main text), as reflect by the slightly larger RMSD values between these images and the intermediate images in the pre-powerstroke state.

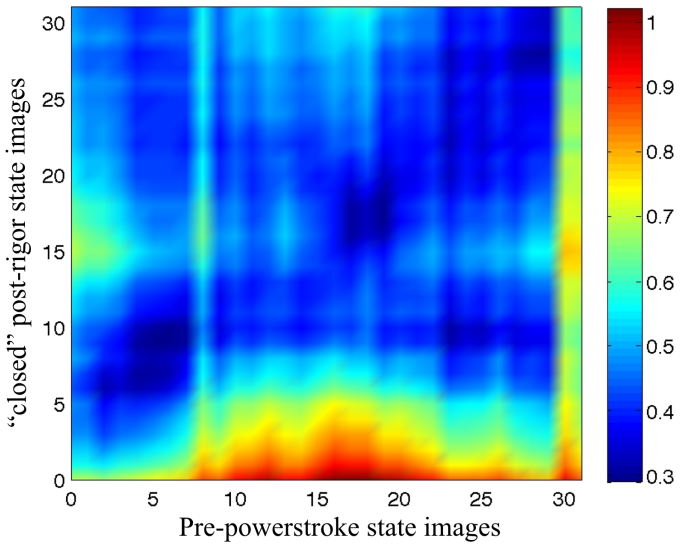

Figure S8: 2D RMSD between the pre-powerstroke state images and the "closed" post-rigor state images

7.3 W2 Pathway in the Pre-powerstroke State

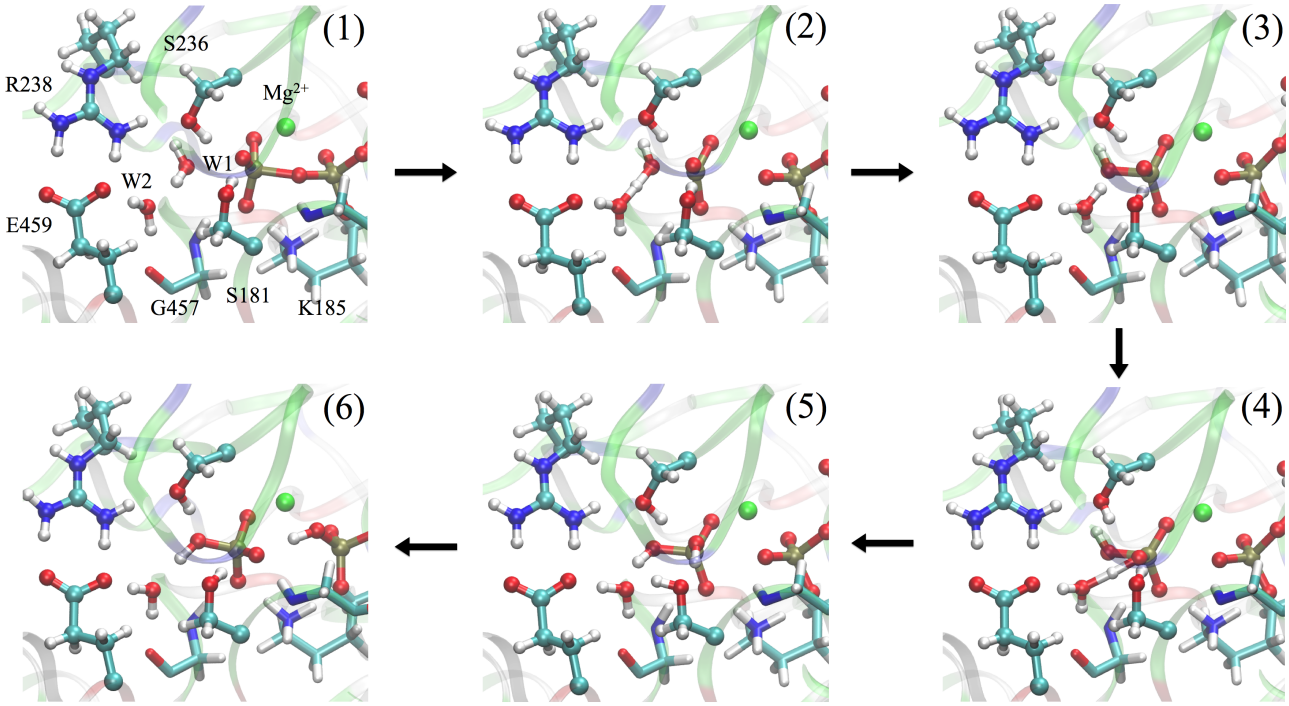

Figure S9: Representative structures along the MFEP obtained from the W2 mechanism in the pre-powerstroke state.

7.4 W2-S181 Pathway in the Pre-powerstroke State

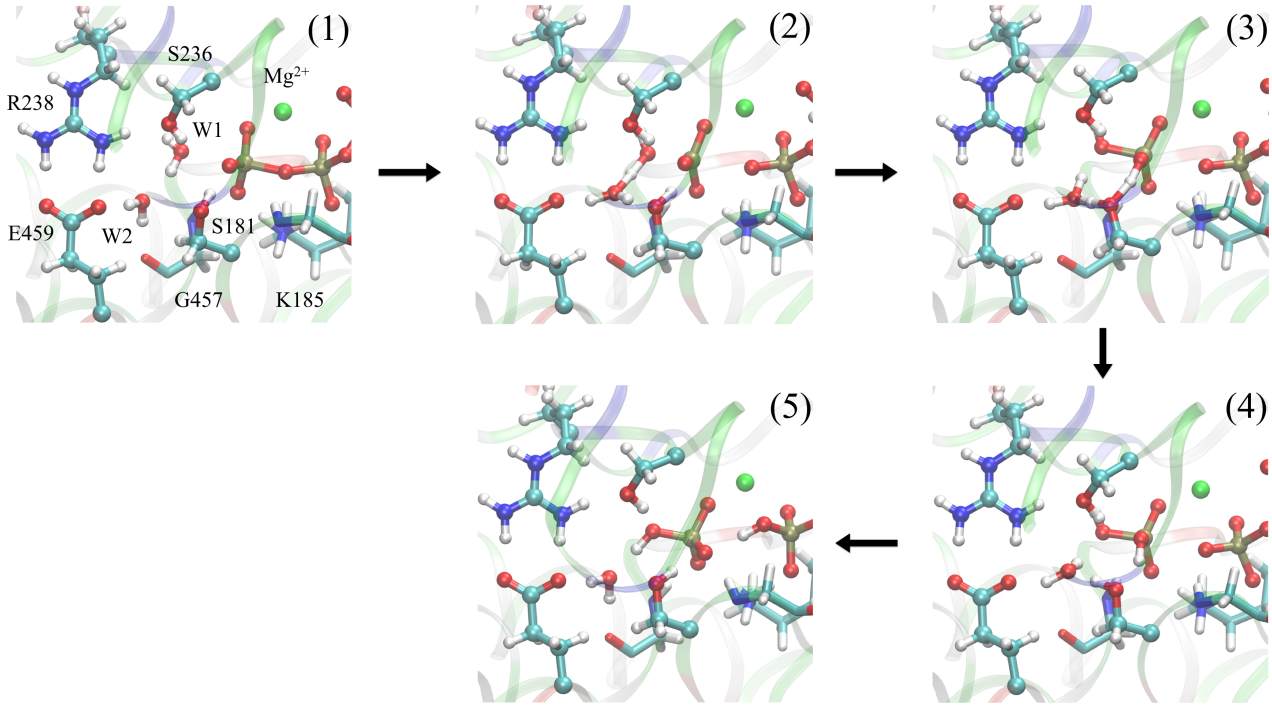

Figure S10: Representative structures along the MFEP obtained from the W2-S181 mechanism in the pre-powerstroke state.

7.5 S236 pathway in the Pre-powerstroke State

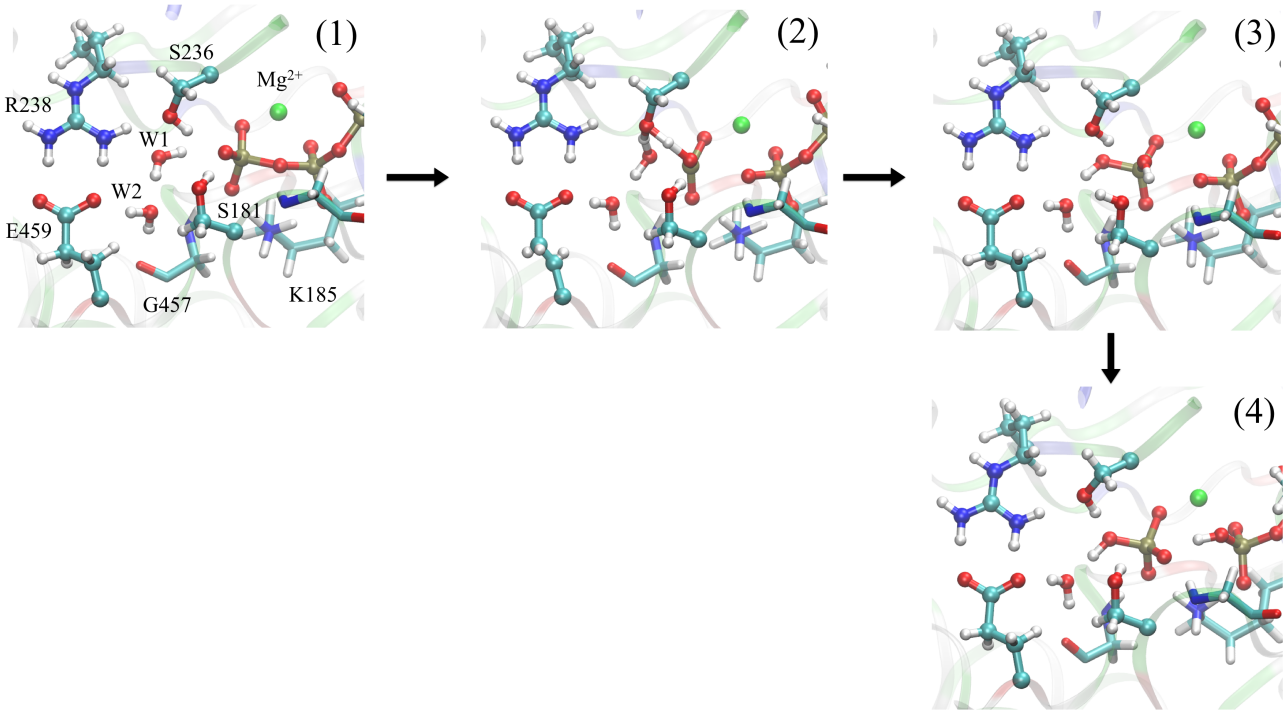

Figure S11: Representative structures along the MFEP obtained from the S236 mechanism in the pre-powerstroke state.

7.6 S236-W3-S181 pathway in the Pre-powerstroke State

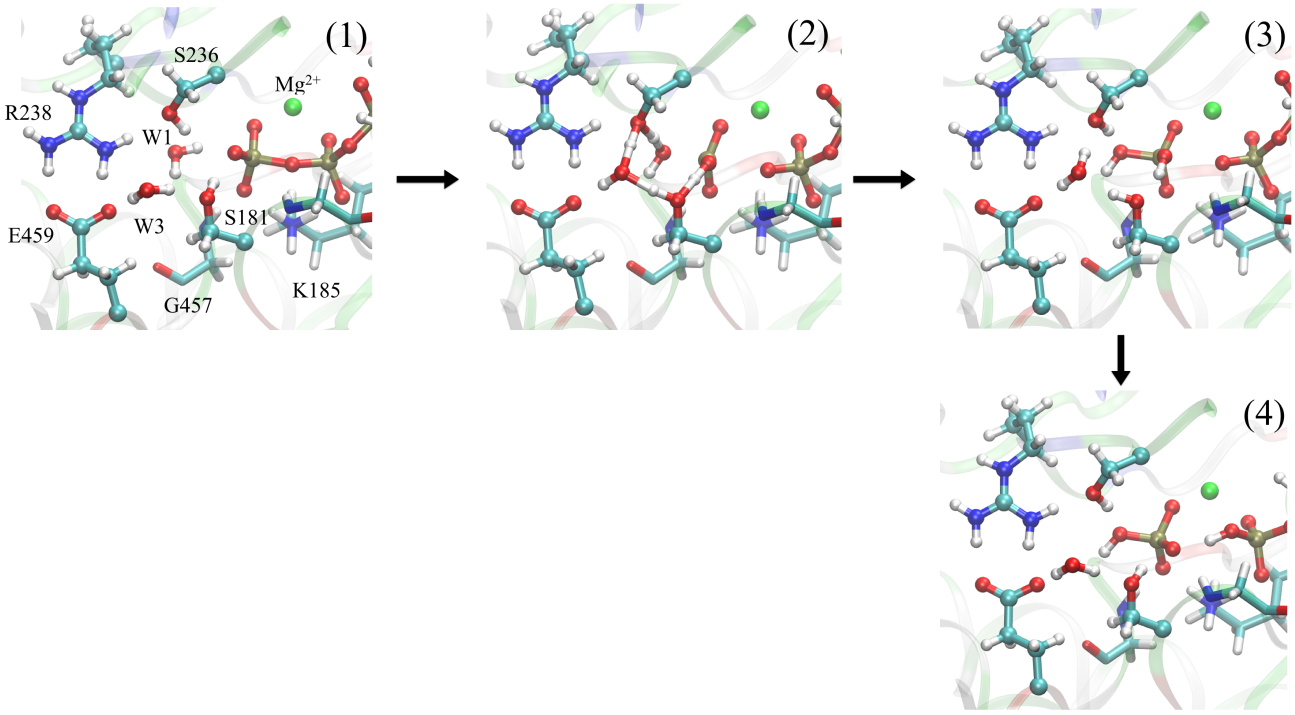

Figure S12: Representative structures along the MFEP obtained from the S236-W3-S181 mechanism in the pre-powerstroke state.

7.7 S236 pathway in the Post-rigor State

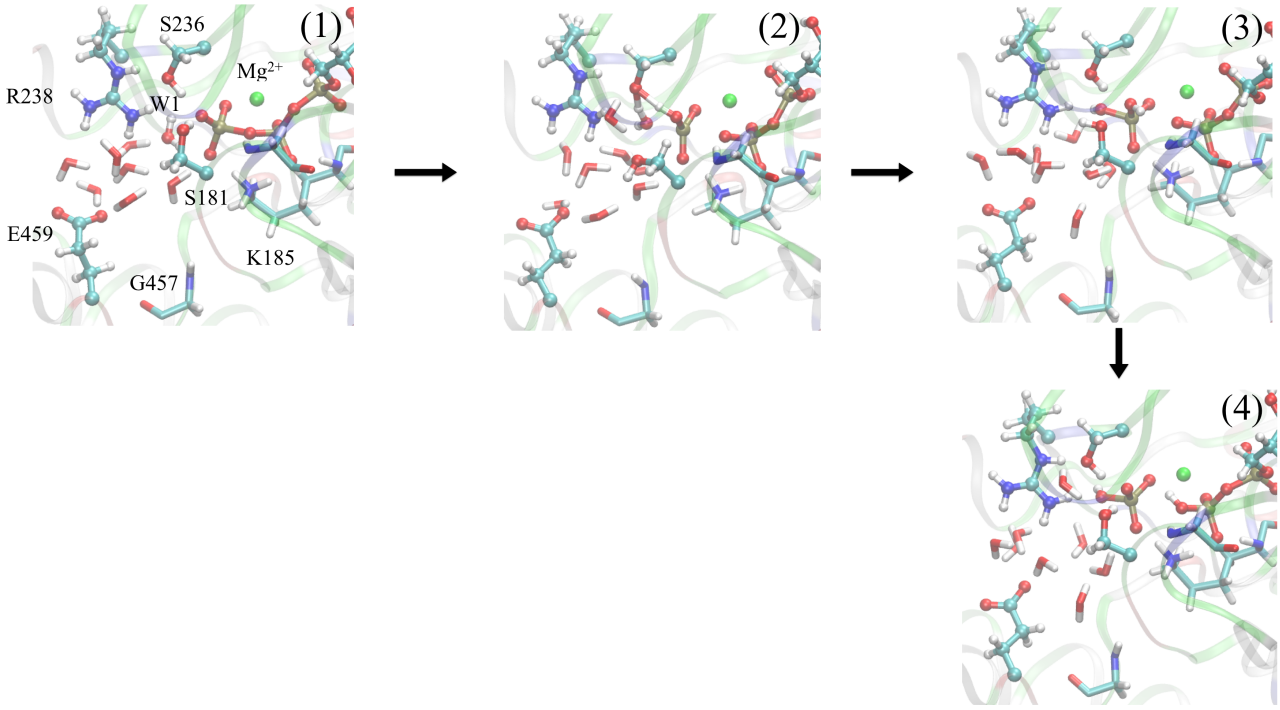

Figure S13: Representative structures along the MFEP obtained from the S236 mechanism in the post-rigor state.

7.8 W2-E459 pathway in the "closed" Post-rigor State

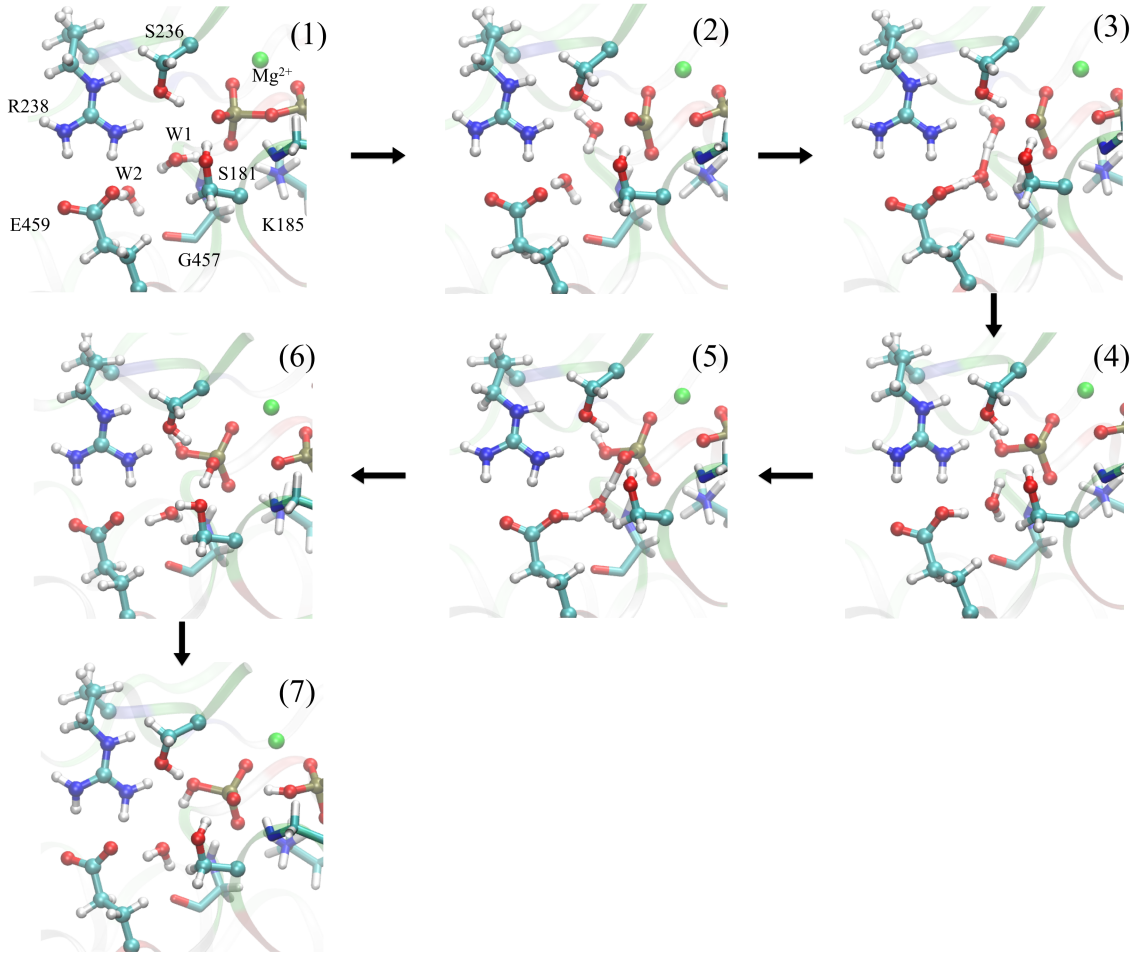

Figure S14: Representative structures along the MFEP obtained from the W2-E459 mechanism in the "closed" post-rigor state.

References

(S1) König, P. H.; Ghosh, N.; Hoffmann, M.; Elstner, M.; Tajkhorshid, E.; Frauenheim, T.; Cui, Q. Toward Theoretical Analyis of Long-Range Proton Transfer Kinetics in Biomolecular Pumps. *J. Phys. Chem. A* **2006**, *110*, 548–563.

(S2) Gaus, M.; Lu, X.; Elstner, M.; Cui, Q. Parameterization of DFTB3/3OB for Sulfur and Phosphorus for Chemical and Biological Applications. *J. Chem. Theory Comput.* **2014**, *10*, 1518–1537.

(S3) Roston, D.; Demapan, D.; Cui, Q. Leaving Group Ability Affects Transition State Structure for Phosphoryl Transfer in a Single Enzyme Active Site. *J. Am. Chem. Soc.* **2016**, *138*, 7386–7394.

(S4) Roston, D.; Cui, Q. Substrate and Transition State Binding in Alkaline Phosphatase Exhibited by Computational Analysis of Isotope Effects. *J. Am. Chem. Soc.* **2016**, *138*, 11946–11957.

(S5) Senn, H. M.; Thiel, W. QM/MM methods for biomolecular systems. *Angew. Chem. Int. Ed.* **2009**, *48*, 1198–1229.

(S6) Cui, Q.; ; Karplus, M. Quantum Mechanics/Molecular Mechanics Studies of Triosephosphate Isomerase-Catalyzed Reactions: Effect of Geometry and Tunneling on Proton-Transfer Rate Constants. *J. Am. Chem. Soc* **2002**, *124*, 3093–3124.

(S7) Riccardi, D.; Schaefer, P.; Yang, Y.; Yu, H.; Ghosh, N.; Prat-Resina, X.; Konig, P.; Li, G.; Xu, D.; Guo, H.; Elstner, M.; Cui, Q. *Feature Article:* Development of effective quantum mechanical/molecular mechanical (QM/MM) methods for complex biological processes. *J. Phys. Chem. B* **2006**, *110*, 6458–6469.

(S8) Zhang, Y. K.; Kua, J.; Mccammon, J. A. Influence of structural fluctuation on enzyme reaction energy barriers in combined quantum mechanical/molecular mechanical studies. *J. Phys. Chem. B* **2003**, *107*, 4459–4463.

(S9) Fischer, S.; Karplus, M. Conjugate peak refinement: an algorithm for finding reaction paths and accurate transition states in systems with many degrees of freedom. *Chem. Phys. Lett.* **1992**, *194*, 252–261.

(S10) Yang, Y.; Yu, H.; York, D.; Elstner, M.; Cui, Q. Description of phosphate hydrolysis reactions with the Self-Consistent-Charge Density-Functional-Tight-Binding (SCC-DFTB) theory 1. Parametrization. *J. Chem. Theory Comput.* **2008**, *4*, 2067–2084.